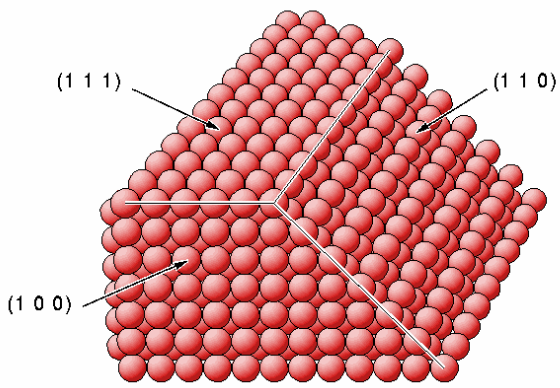
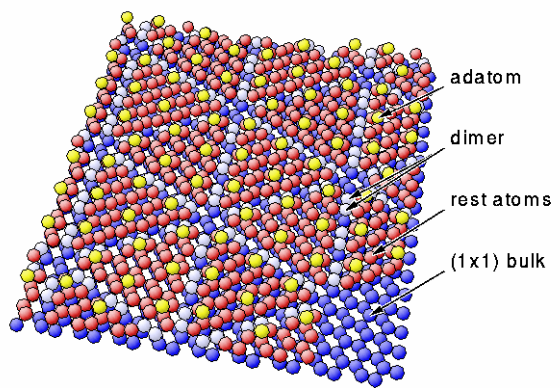


表面とは？



fcc lattice : different net planes

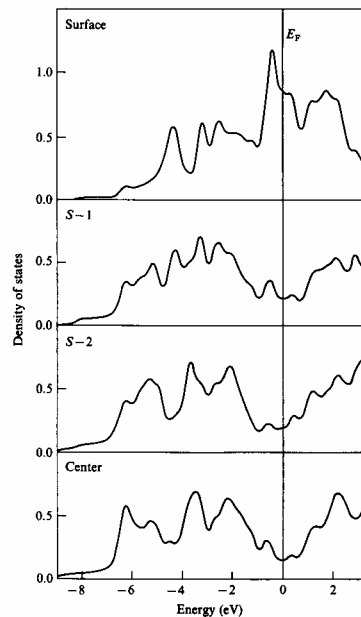
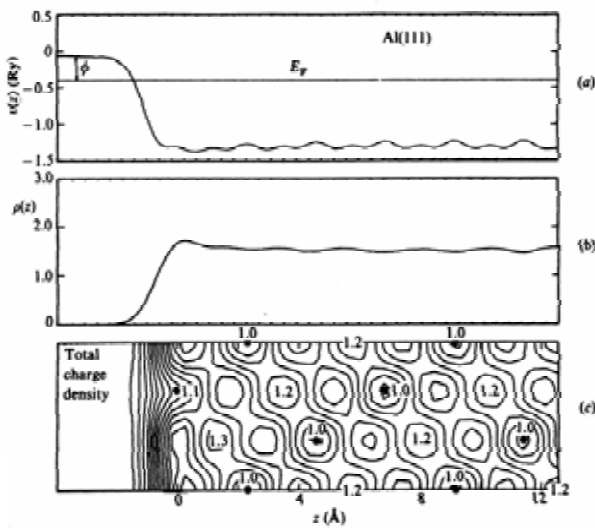


Si(111)-(7x7) DAS model (Takayanagi/Tong)

BA1,SAC pl4

Fig. 4.25. Slab calculation of layer-resolved LDOS for W(100). Surface states 'fill in' the bulk LDOS (Posternak, Krakauer, Freeman & Koelling, 1980).

Fig. 4.23. Surface electronic properties of Al(111): (a) effective potential; (b) electron density profile; (c) charge density contours (Chelikowsky, Schluter, Louie & Cohen, 1975).



どのように見る？

表1-2 代表的な表面測定手法と得られる知見

得られる知見	表面測定手法	バルクの測定手法
原子配列 結晶構造	低速電子回折 (LEED) 反射高速電子回折 (RHEED) 透過電子回折 (TED) 表面 X 線回折 (SXD) 直衝突イオン散乱分光 (ICISS) 走査トンネル顕微鏡 (STM) <u>原子間力顕微鏡 (AFM)</u>	電子回折 X 線回折 中性子回折 NMR
化学組成	<u>オージェ電子分光 (AES)</u> 2 次イオン質量分析 (SIMS)	発光分析 蛍光 X 線分析
電子構造 結合様式	紫外光電子分光 (UPS) <u>X 線光電子分光 (XPS, ESCA)</u> エネルギー損失分光 (ELS) 走査トンネル分光 (STS)	光学吸収 光学反射
原子振動	高分解能エネルギー損失分光 (HREELS) 全反射赤外分光 (ATR-IR)	赤外吸収 ラマン分光
磁性	磁気力顕微鏡 (MFM) スピン偏極走査電子顕微鏡 (SP-SEM)	帯磁率測定 ESR

$$\Gamma = \frac{1}{4V} n \bar{v} dS$$

(molm⁻³)(ms⁻¹)

$$PV = nRT$$

$$\bar{v} = \sqrt{\frac{8RT}{\pi M}}$$

1 atm = 760 Torr
= 101325 Pa
1 Torr = 133.3 Pa

$$= \sqrt{\frac{8 \times 8.314 \times 300}{\pi \times 28 \times 10^{-3}}}$$

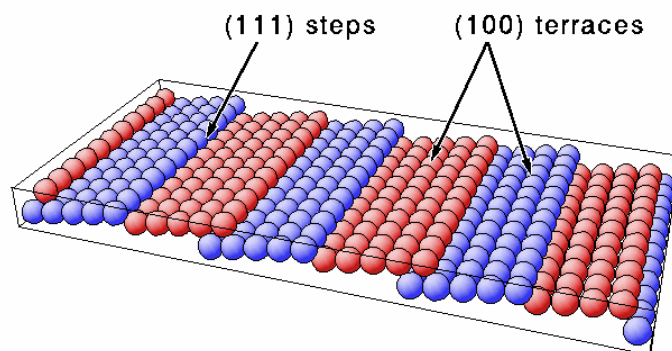
$$= 464 \text{ (ms}^{-1}\text{)}$$

$$dS = (3 \times 10^{-10})^2 = 10^{-19}$$

$$\frac{n}{V} = \frac{P}{RT}$$

10⁻⁶ Torr 1層覆うのに何秒?
!0⁻¹⁰ Torr

平均自由行程 $\lambda [10^{-5} \text{m}] = 5/P [\text{Torr}]$



表面に敏感？

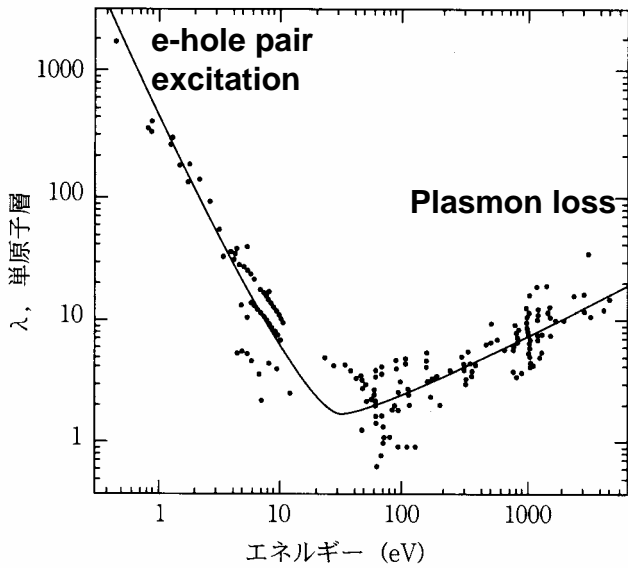


図 2-6 物質中での電子の飛程の運動エネルギー^[9]

AESは軽元素？

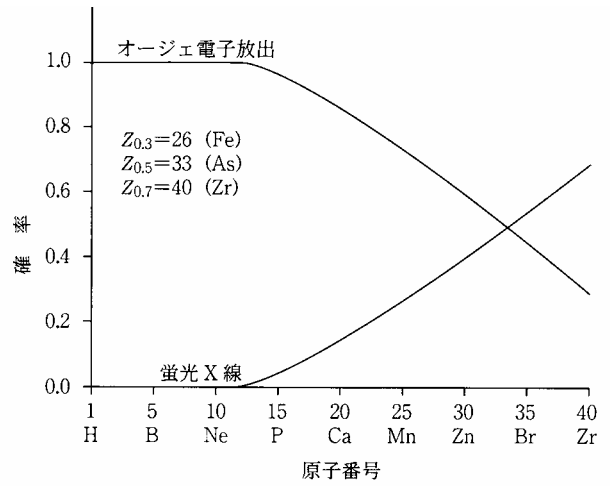
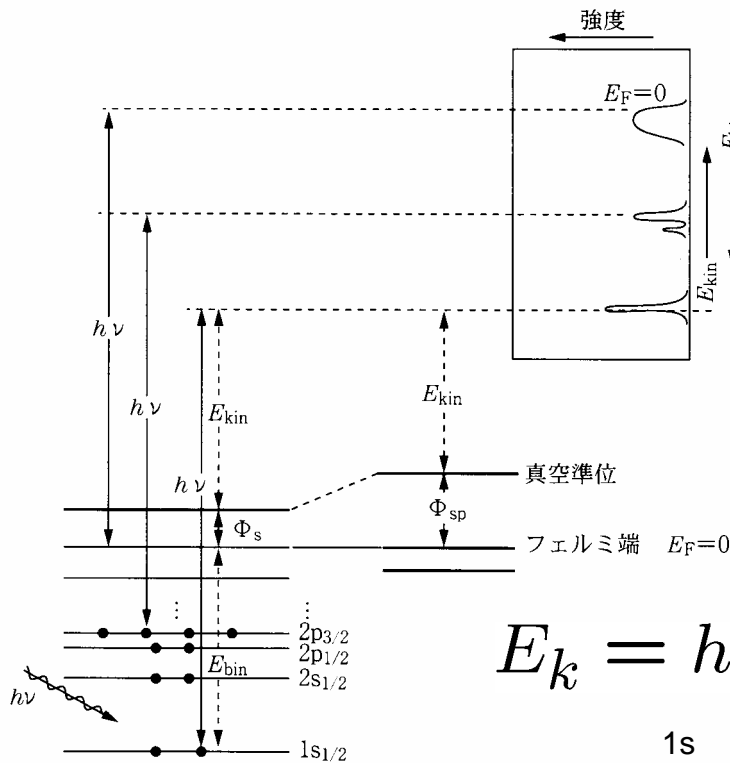


図 2-2 K 殻の電子が放出された後のオージェ電子励起と特性 X 線放出の相対確率の原子番号依存性^[1]

Mg K
1250 eV



$$E_k = h\nu - E_b - \Phi$$

	1s	2s	2p _{1/2}	2p _{3/2}
12 Mg	1303.0+			
16 S	2472	230.9	163.6*	162.5*

図 2-15 XPS の原理

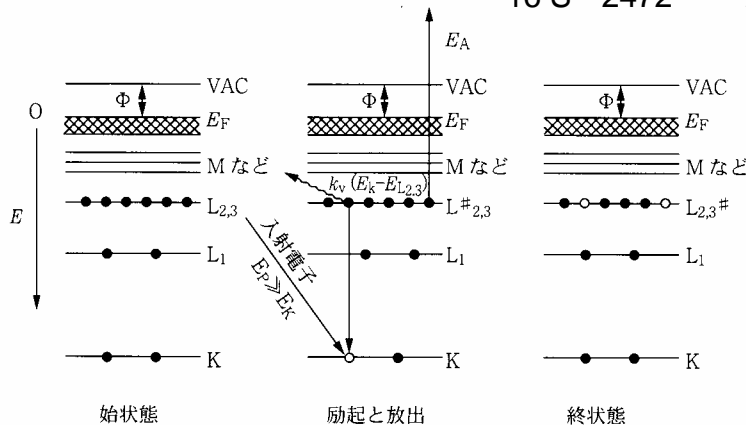


図 2-1 オージェ電子生成の概念図

Fig. 1. The xps experiment.

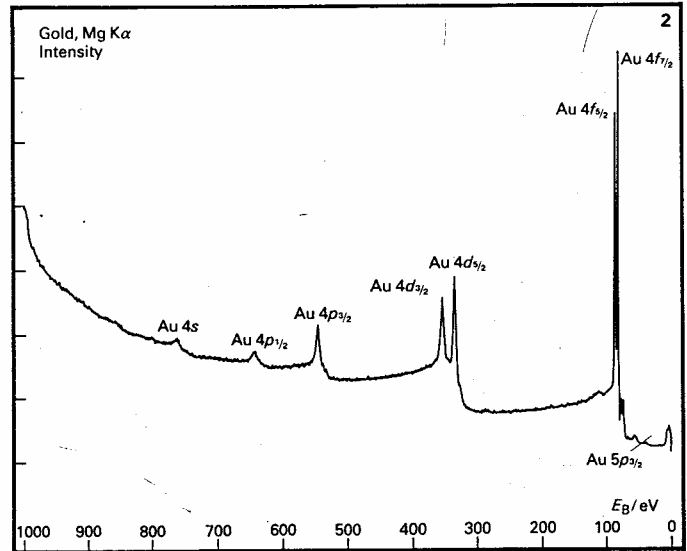
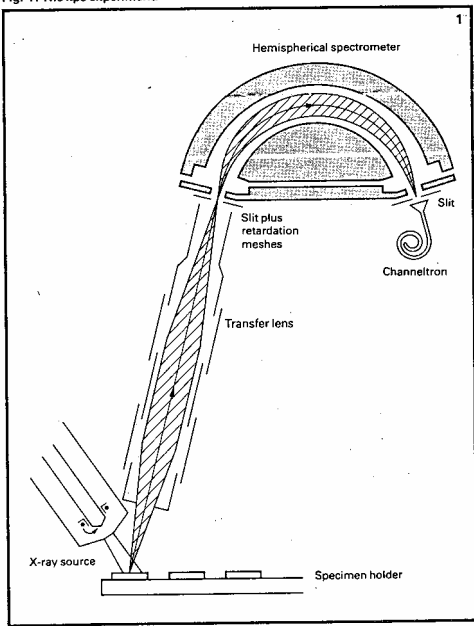


Fig. 2. The gold xps spectrum using MgK α radiation.³

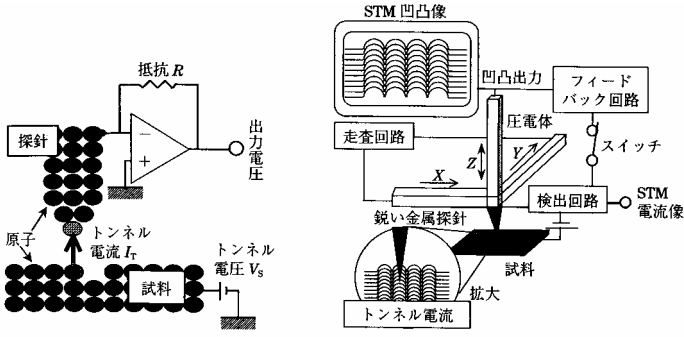


図 2.1 局所的トンネル電流測定
の原理

図 2.2 走査型トンネル顕微鏡の原理



Exact copy of first Scanning Tunneling Microscope of Binnig and Rohrer (original have not preserved).

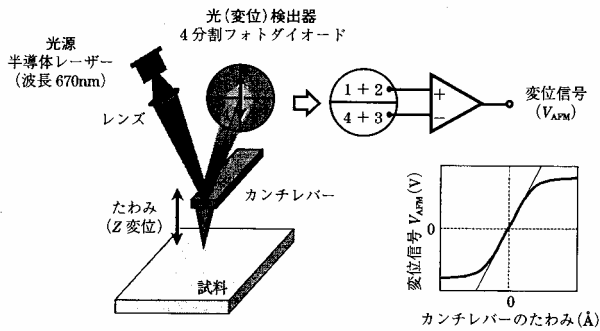
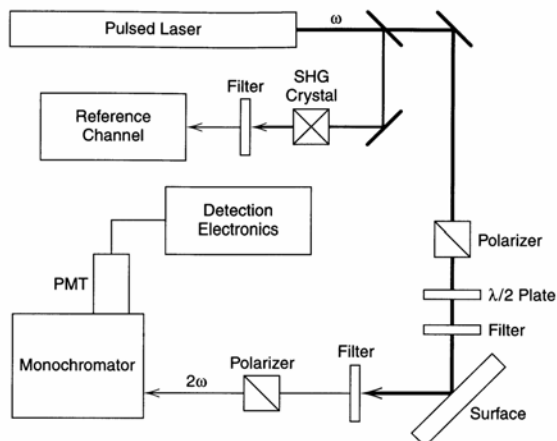


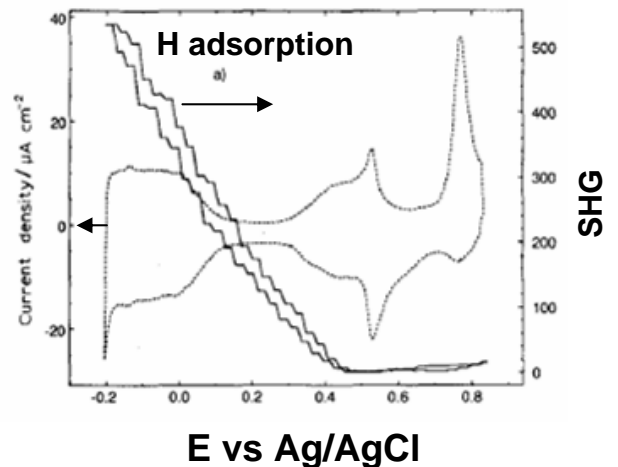
図 2.9 カンチレバーの変位検出計 (光てこ方式)

**電気化学：電流vs電圧曲線
界面現象(nm) 物質移動・電子移動**

非線形表面分光(SHG,SFG)



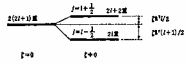
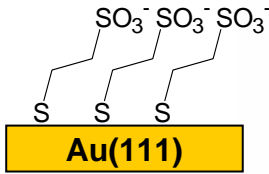
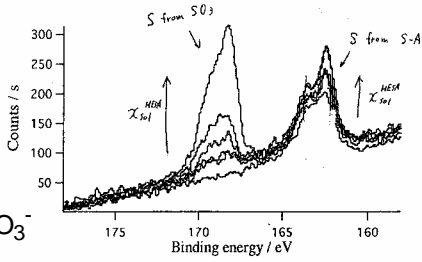
SHG Pt(111) 0.1 M HClO₄



表面分析 機器分析化学

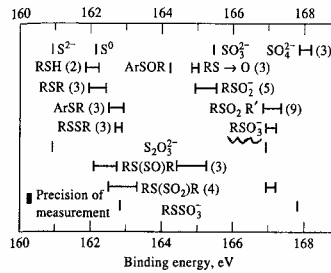
XPS

XPS data from MESA (Hobara 2000 6/30)
The binding energies of photoelectron from the S atom in the S-Au bonds are ca. 162 eV, which are independent of the terminal functional groups of the SAM.



Skoog et al. "Principles of Instrumental Analysis"

2p_{1/2} = 163.6 eV
2p_{2/3} = 162.5 eV



Correlation chart for sulfur 2p electron binding energies. The numbers in parentheses indicate the number of compounds examined. (Reprinted with permission from D. M. Hercules, Anal. Chem., 1970, 42(1), 35A. Copyright 1970 American Chemical Society.)

STM (C. J. Chen, Introduction to STM, Oxford 1993)

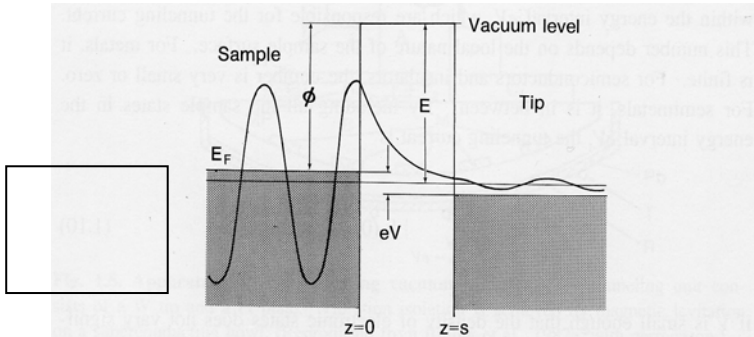


Fig. 1.4. A one-dimensional metal-vacuum-metal tunneling junction. The sample, left, and the tip, right, are modeled as semi-infinite pieces of free-electron metal.

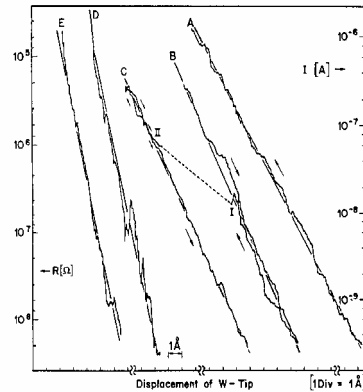
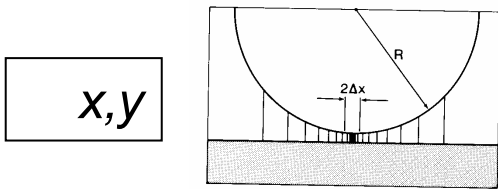


Fig. 1.6. Tunneling through a controllable vacuum gap. The exponential dependence $I \sim V$ is observed over four orders of magnitude. On clean surfaces, an apparent barrier height of 3.5 eV was observed. (Reproduced from Binnig et al., 1982a, with permission.)



R=1000 , $\chi = 45$

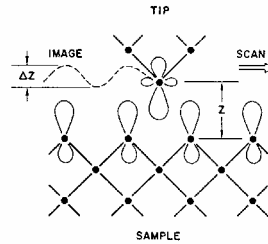
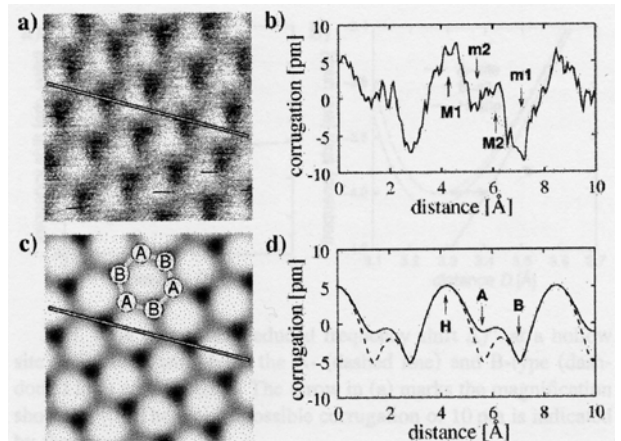
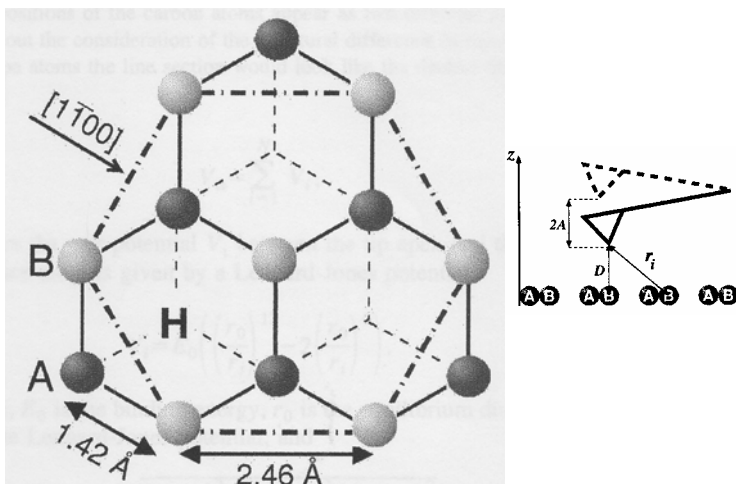
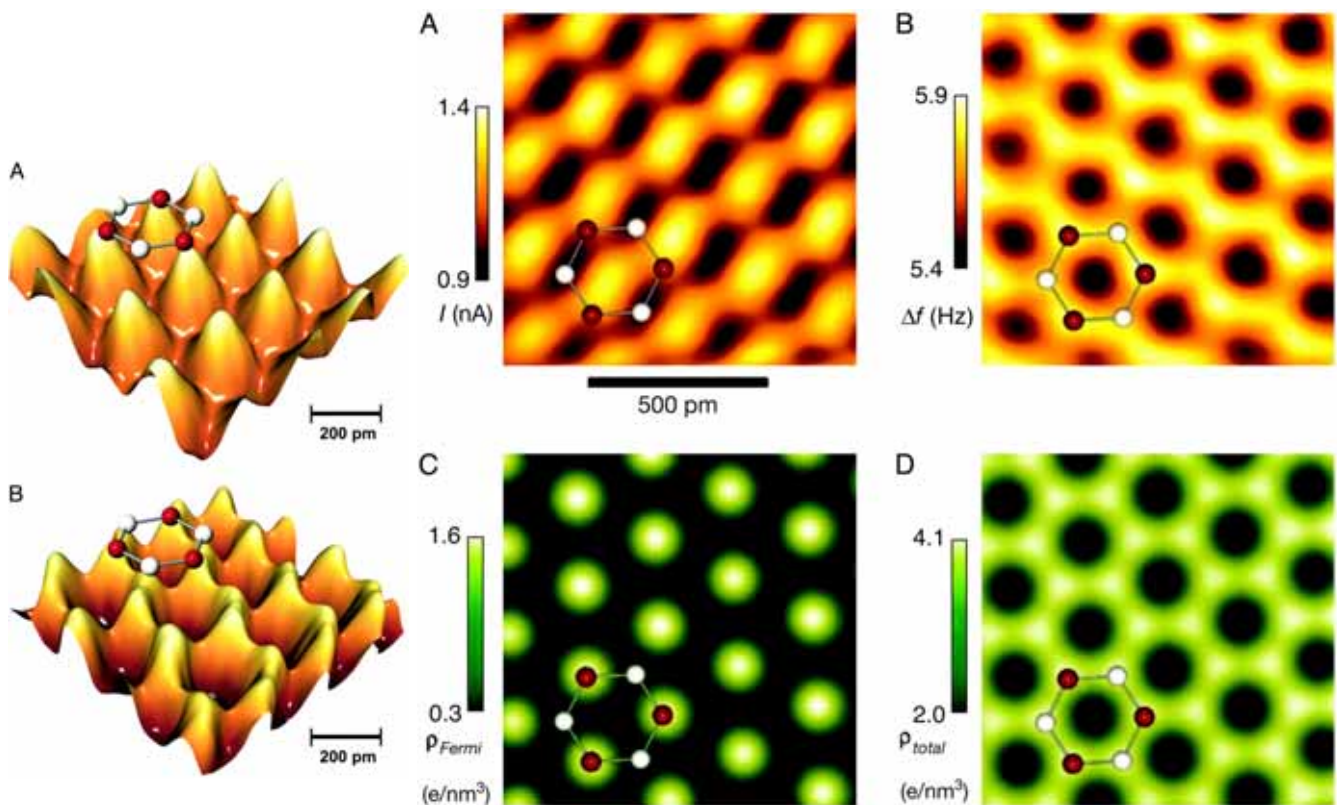
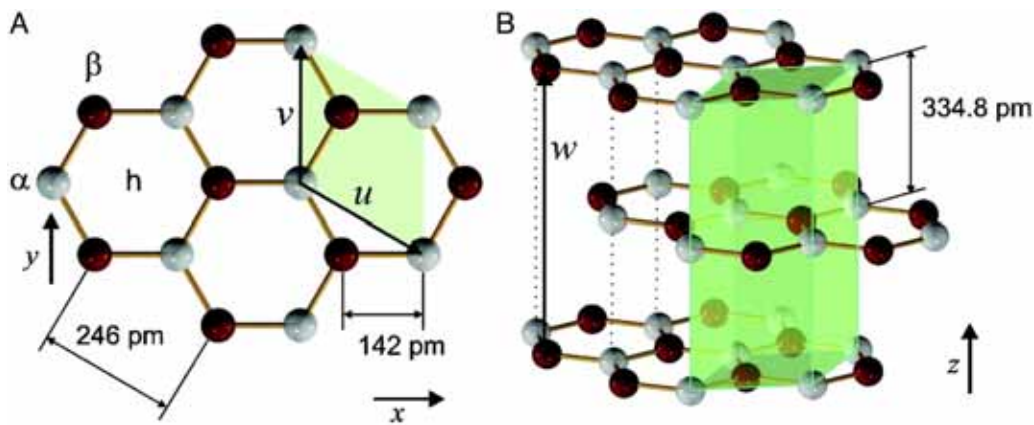


Fig. 1.28. Microscopic view of STM imaging mechanism. An atomic state at the tip end, exemplified by a d state protruding from the apex of a W tip, interacts with a two-dimensional array of atomic states, exemplified by sp³ states on the Si surface. This results in a highly corrugated tunneling current distribution. (Reproduced from Chen, 1991, with permission.)

AFM (H. Holsher et al. PRB 2000 62, 6967-6970)





Missing carbon atoms of Graphite in STM

Experimental and simulated STM and AFM images of graphite. One hexagonal surface unit cell with the two basis atoms (white) and (red) is superimposed for clarity. (A) Experimental image of graphite in constant-height dynamic STM mode (bias voltage +100 mV, amplitude 300 pm, scanning speed 0.2 nm/s). The tunneling current ranges from 0.9 to 1.4 nA. Only the α atoms appear in the image. The green arrow indicates a shift of the experimental STM image with respect to the AFM image by 68 pm (see text). (B) Experimental image of graphite in constant-height dynamic AFM mode showing both α and β atoms. The frequency shift data have been recorded simultaneously with the tunneling data shown in A, ranging from +5.4 to +5.9 Hz. (C) The calculated charge density of graphite at the Fermi level ρ_{Fermi} (after refs. 11 and 12) at a height of 200 pm over the surface plane, ranging from 0.3 to 1.6 electrons per nm³. The maxima of ρ_{Fermi} are at the α atom positions. The STM image reflects the charge density at the Fermi level. (D) Calculated total charge density, also at a height of 200 pm over the surface plane, ranging from 2.0 to 4.1 electrons per nm³. The repulsive forces that are imaged in the experimental AFM image (B) are increasing with the charge density; thus, a charge density plot is a good approximation for a repulsive AFM image. The experimental image in B and the calculated charge density shown in D have local maxima over α and β sites.

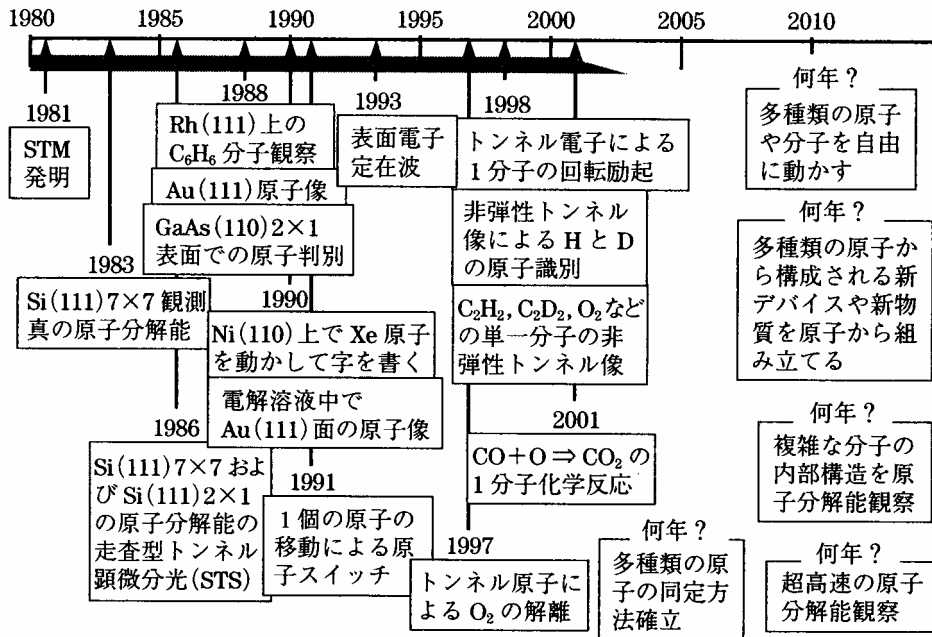


図 2.7 STM の歴史, 現状, 将来

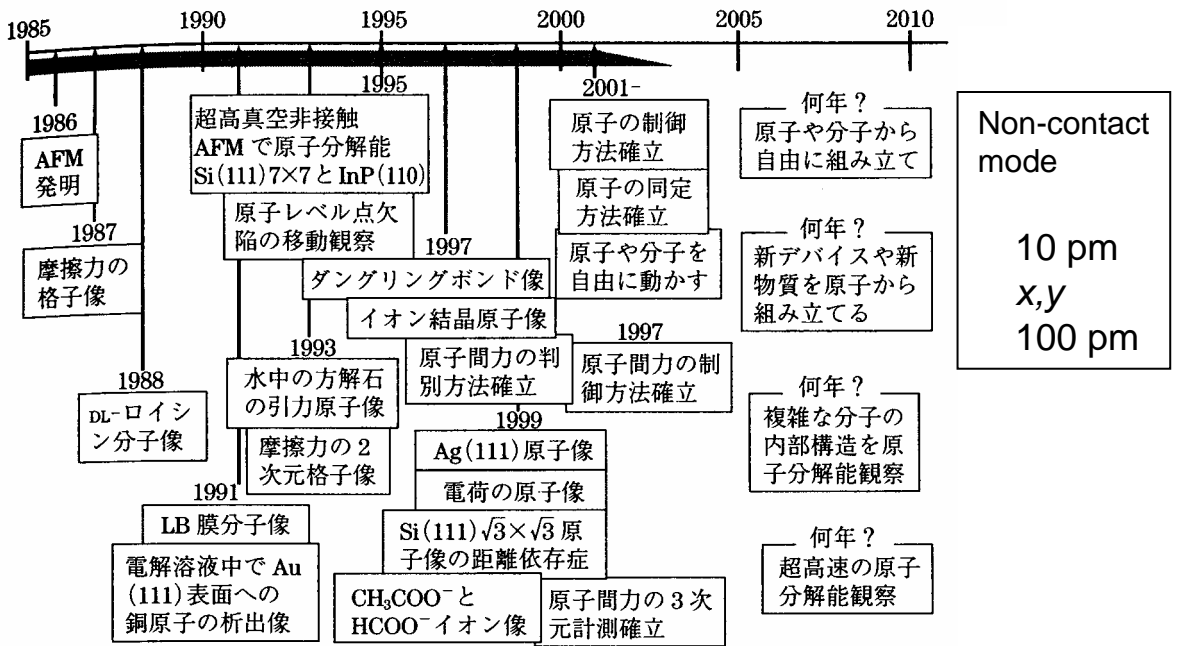
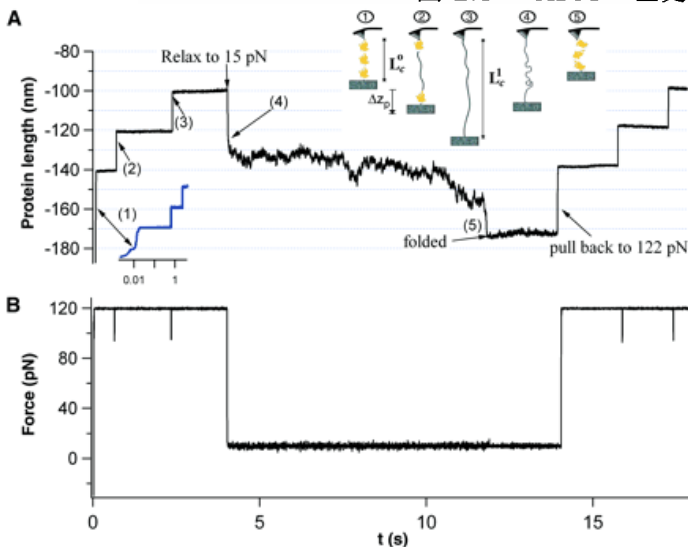
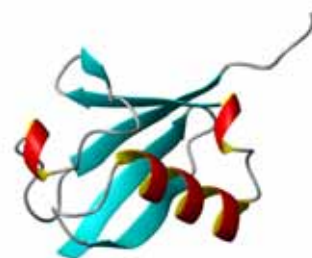


図 2.8 AFM の歴史, 現状, 将来



Science, Vol 303, 1674-1678, 2004
Force-Clamp Spectroscopy Monitors the Folding Trajectory of a Single Protein
 Julio M. Fernandez* and Hongbin Li

Fig. 1. The folding pathway of ubiquitin is directly measured by force-clamp spectroscopy.



表面科学の実験的手法

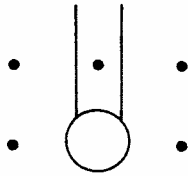
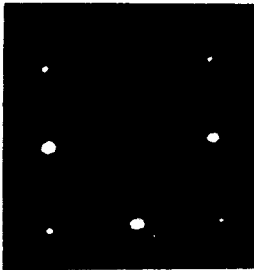
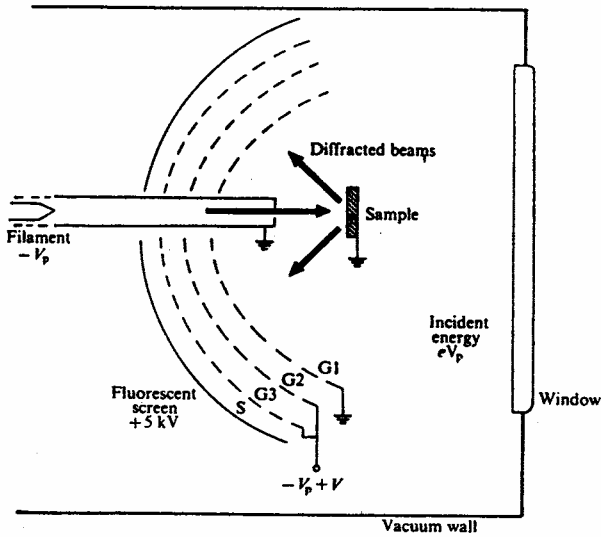
1. 表面構造

回折法 LEED Low Energy Electron Diffraction
 RHEED Reflection High Energy Electron Diffraction
 TED Transmission Electron Diffraction

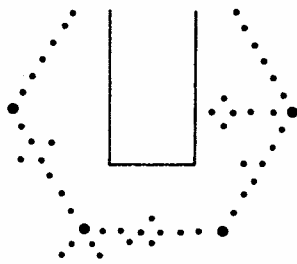
表面顕微鏡

SEM Scanning Electron Microscope
 STM Scanning Tunneling Microscope
 AFM Atomic Force Microscope

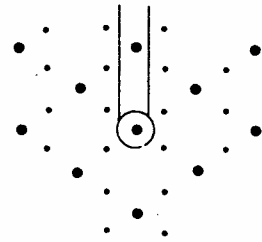
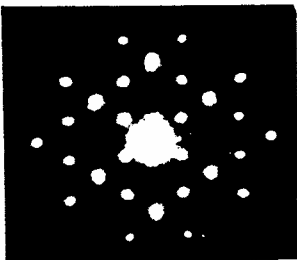
測定例



(a)

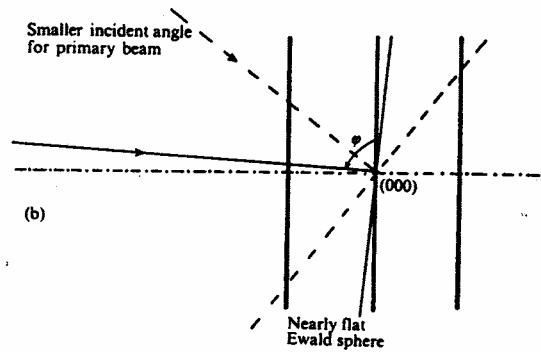
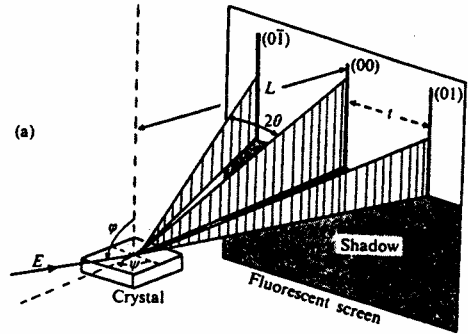


(b)

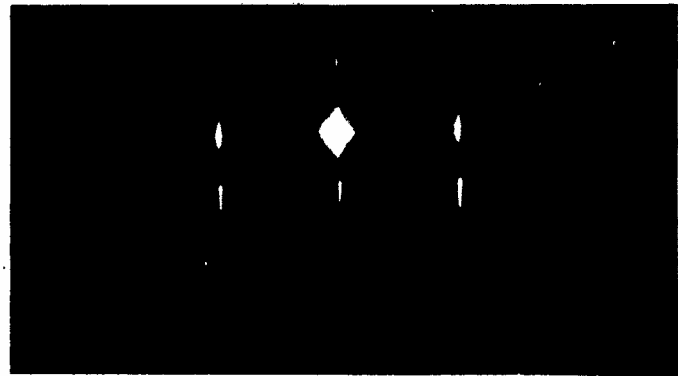


(c)

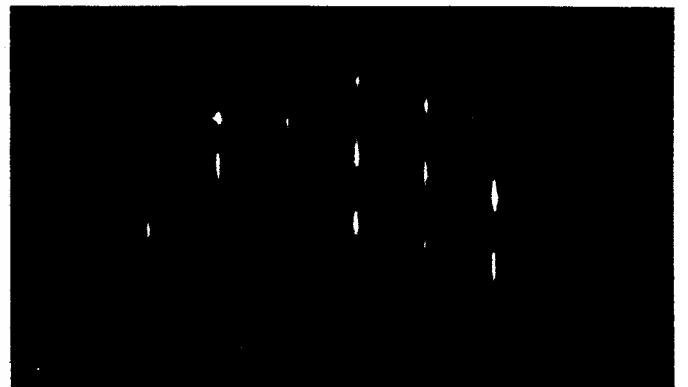
Some typical LEED patterns. (a) The clean Cu(100) surface. Only spots from the bulk exposed plane are present. Primary energy 150 eV. (By courtesy of Dr R. J. Reid, New University of Ulster.) (b) The clean Si(111) surface. Extra spots are present between the six (10) features (bright spots) from the bulk exposed plane. These extra features correspond to a surface mesh parallel to the substrate mesh but with 7 times the length of its sides. Because of these $\frac{1}{7}$ th order spots this pattern is called Si(111)(7 x 7) or Si(111)7. Primary energy 42 eV. (c) The W(110)-(2 x 1)-O LEED pattern due to oxygen adsorbed on W(110). Primary energy 53 eV. (By courtesy Dr J. W. May, Eastman-Kodak Laboratories, New York.)



The RHEED method. (a) Experimental geometry. A fine parallel beam of electrons is incident near $\phi = 90^\circ$ upon a flat single-crystal surface. (b) Ewald sphere construction for RHEED.

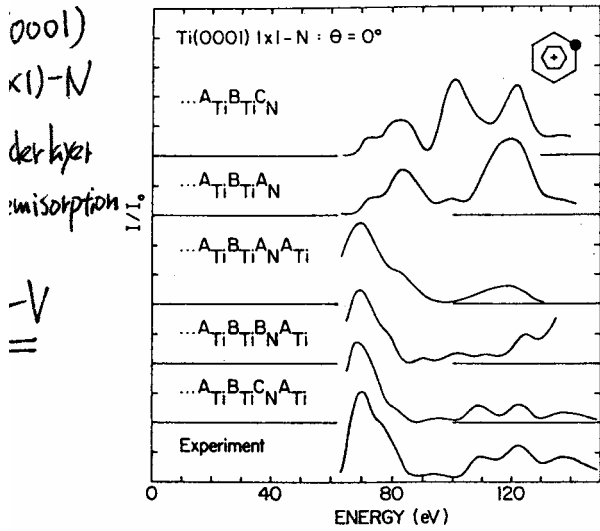


(a)

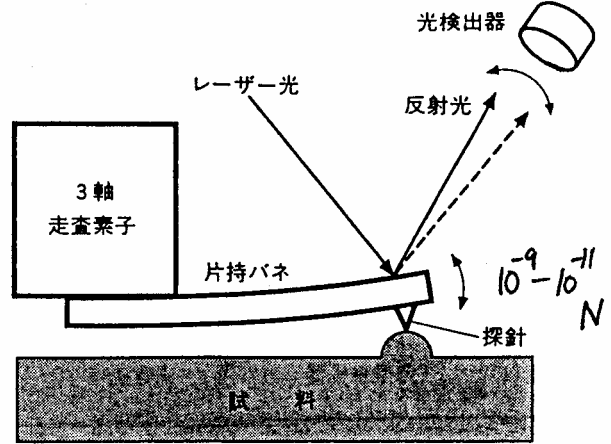


(b)

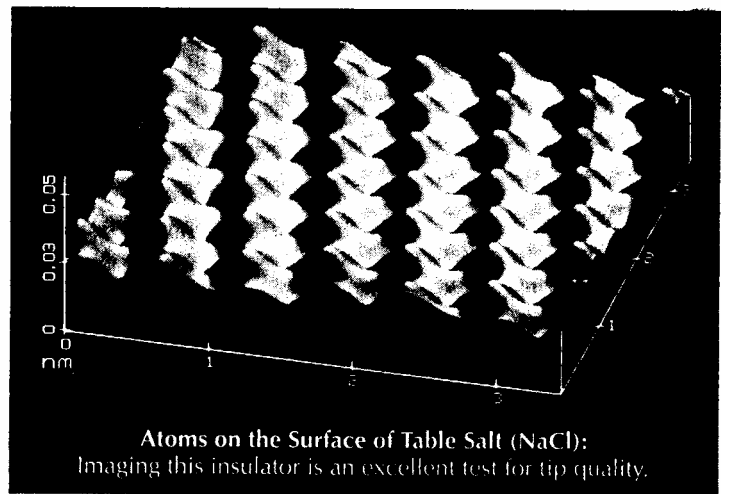
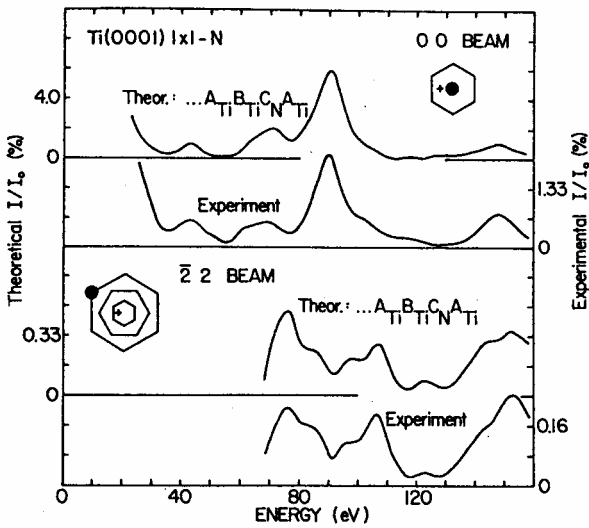
RHEED patterns obtained at 100 keV from the (111) surface of silicon (a) $[\bar{2}11]$ azimuth; (b) $[101]$ azimuth. The streaking indicates that the surface is flat.



STM 絶縁層 < 2 nm 除震 画像処理



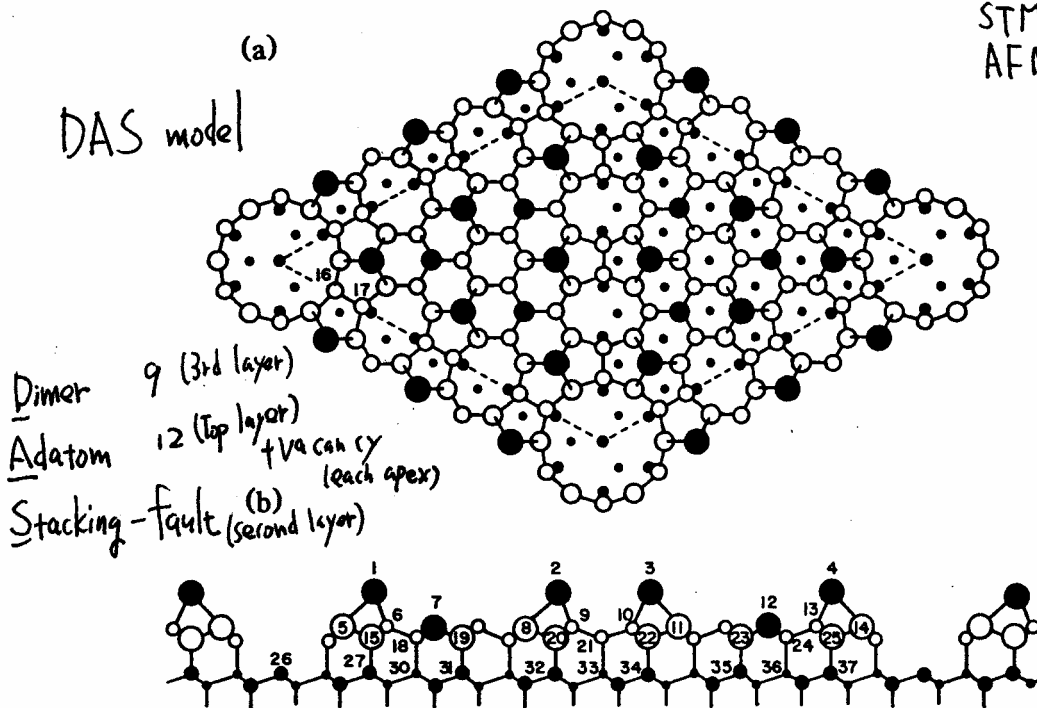
原子間力顕微鏡 (AFM) の構成.



p(0001), fcc(111) (2x2) ↔ (2x1)₃ domains structure

分解能	X	Z
STM	0.1 nm	0.01 nm
AFM	0.2 nm	0.1 nm

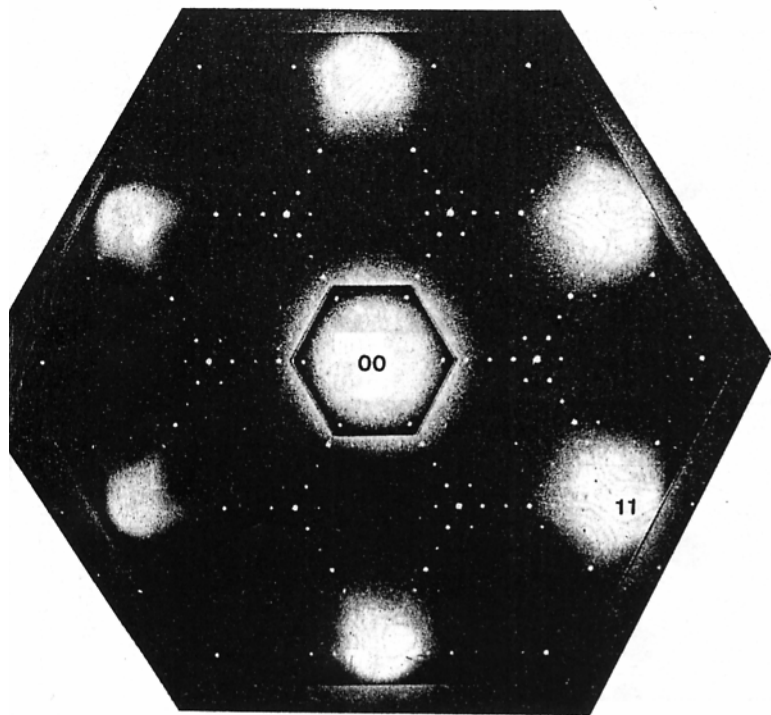
(a)
 DAS model



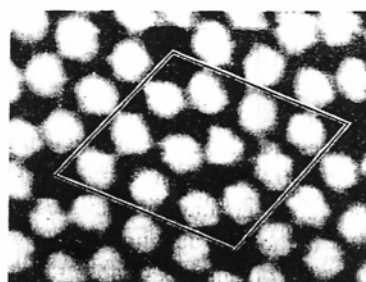
dangling bond
 49
 ↓
 19

(a) Top view of the DAS model for the Si(111)-(7x7) surface reconstruction. The (7x7) unit cell is outlined. Atoms at increasing distances from the surface are indicated by circles of decreasing size. The large solid circles denote the twelve adatoms. The smaller solid circles represent the rest atoms. The faulted half of the unit cell is on the left. Small open circles denote the dimers, while small solid circles and dots represent atoms in the unreconstructed layers. (b) Side view. Atoms on the lattice plane along the long diagonal of the surface unit cell are shown with larger circles than those behind them. The numbers label the 37

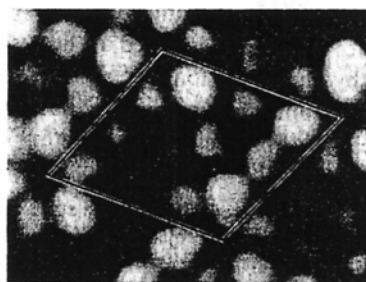
Transmission electron diffraction pattern for Si(111) 7×7 (Takayanagi *et al.*, 1985).



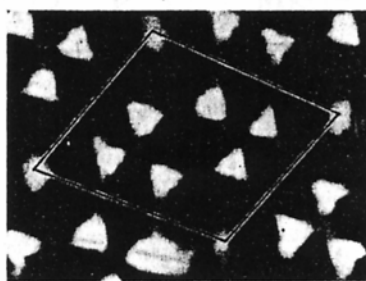
Scanning tunnelling microscopic images of the topogra (top panel) and three electronic surface states of a Si(111) 7×7 surface. See text for discussion (Hamers, Tromp & Demuth, 1986)



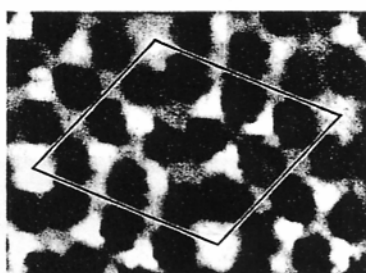
STM



0.35 eV
below E_F

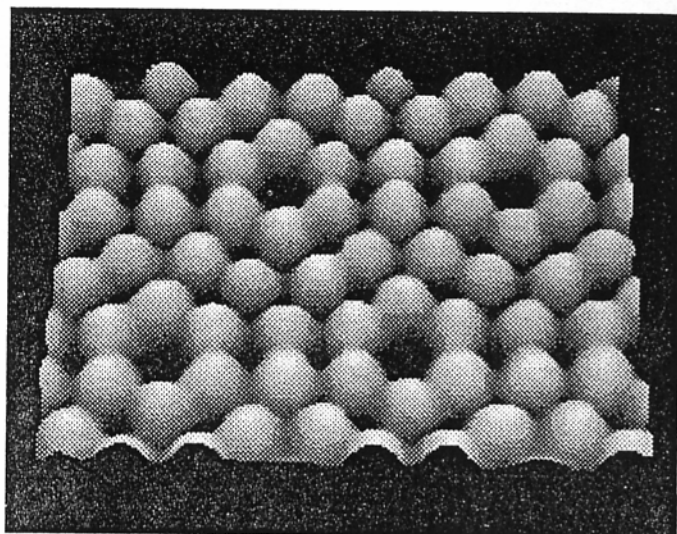
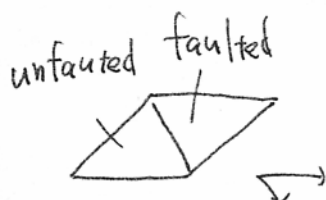
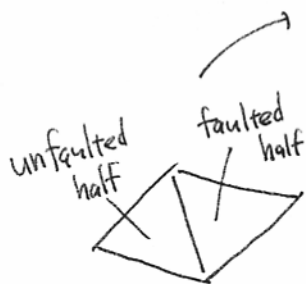


0.8 eV
below E_F
(dangling bonds
of the six
second layer)
+ corner holes

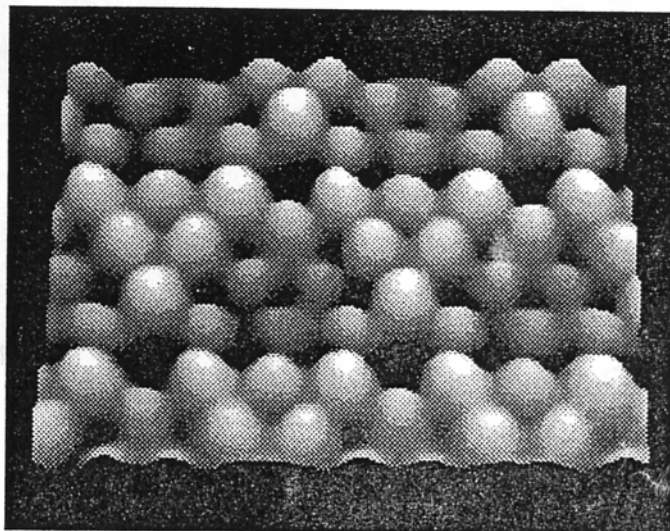


1.8 eV
below E_F

adatom $3p_{x,y}$
direct \downarrow
below $3p_z$
adatom



unoccupied states
針 \rightarrow Si(111)



occupied states
STM

For rutile $\text{TiO}_2(110)$ surface, atomic-resolution STM is only successful when imaging unoccupied state(positive bias) on slightly reduced(n-type) samples.

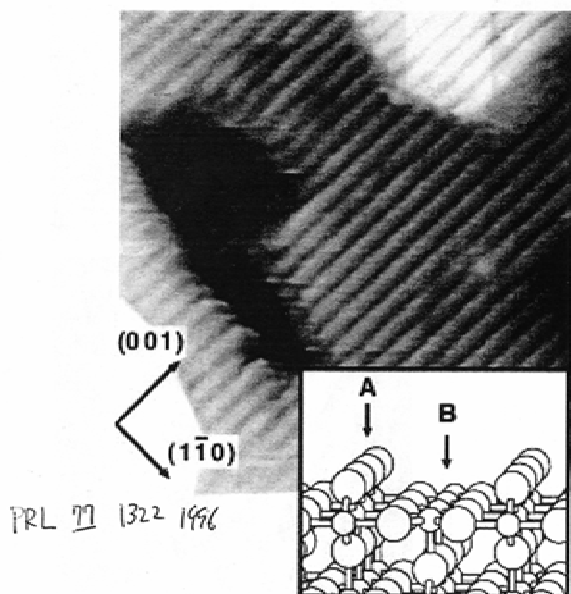


FIG. 1. STM image of a stoichiometric 1×1 $\text{TiO}_2(110)$ surface, $140 \times 140 \text{ \AA}^2$. Sample bias +1.6 V, tunneling current 0.38 nA. The inset shows a ball-and-stick model of the unrelaxed 1×1 $\text{TiO}_2(110)$ surface. Rows of bridging oxygen atoms are labeled "A," rows of fivefold coordinated titaniums "B."

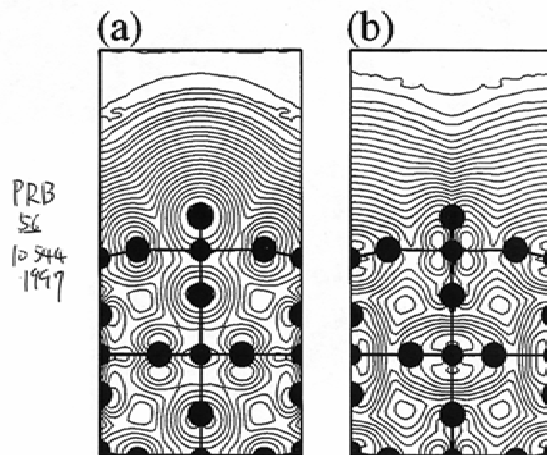
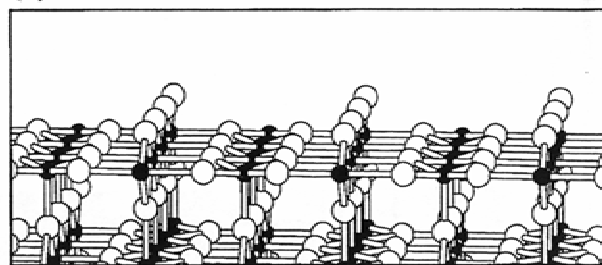


FIG. 2. (a) Contour plots of $[001]$ -averaged charge densities for the relaxed stoichiometric 1×1 surface. (a) Near-VBM charge densities obtained by integrating the LDOS over a 1-eV energy window near the valence band maximum. (b) Near-CBM charge densities obtained by integrating over a 2-eV energy window near the conduction band minimum. Contour levels correspond to a geometric progression of charge density, with a factor of 0.56 separating neighboring contours.

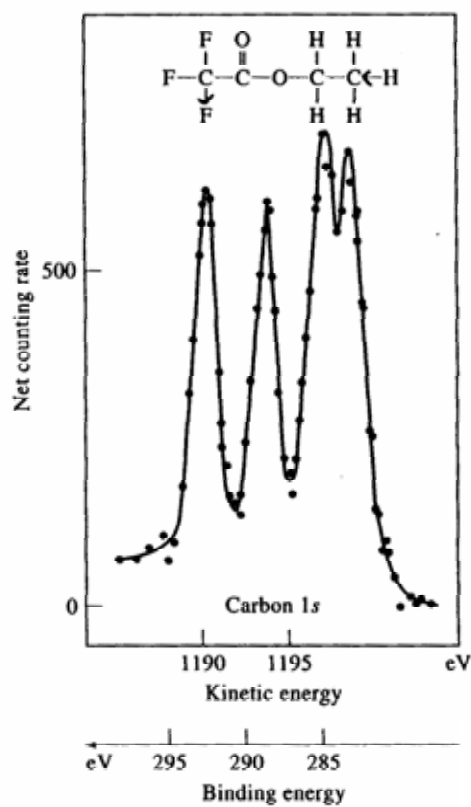


Figure 21-5 Carbon 1s X-ray photoelectron spectrum for ethyl trifluoroacetate. (From K. Siegbahn et al., ESCA: Atomic, Molecular, and Solid-State Studies by Means of Electron Spectroscopy, p. 21. Upsala: Almqvist and Wiksells, 1967. With permission.)

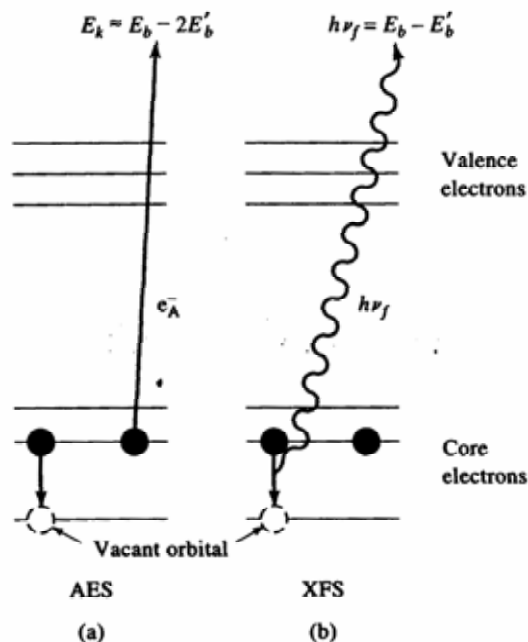


Figure 21-7 Schematic representation of the source of (a) Auger electron emission and (b) X-ray fluorescence that competes with Auger emission.

1.2 Tunneling: an elementary model

In this section, we discuss the concept of tunneling through an elementary one-dimensional model. In classical mechanics, an electron with energy E moving in a potential $U(z)$ is described by

$$\frac{p_z^2}{2m} + U(z) = E, \quad (1.1)$$

where m is the electron mass, 9.1×10^{-28} g. In regions where $E > U(z)$, the electron has a nonzero momentum p_z . On the other hand, the electron cannot penetrate into any region with $E < U(z)$, or a *potential barrier*. In quantum mechanics, the state of the same electron is described by a wavefunction $\psi(z)$, which satisfies Schrödinger's equation,

$$-\frac{\hbar^2}{2m} \frac{d^2}{dz^2} \psi(z) + U(z)\psi(z) = E\psi(z). \quad (1.2)$$

Consider the case of a piecewise-constant potential, as shown in Fig. 1.3. In the classically allowed region, $E > U$, Eq. (1.2) has solutions

$$\psi(z) = \psi(0)e^{\pm ikz}, \quad (1.3)$$

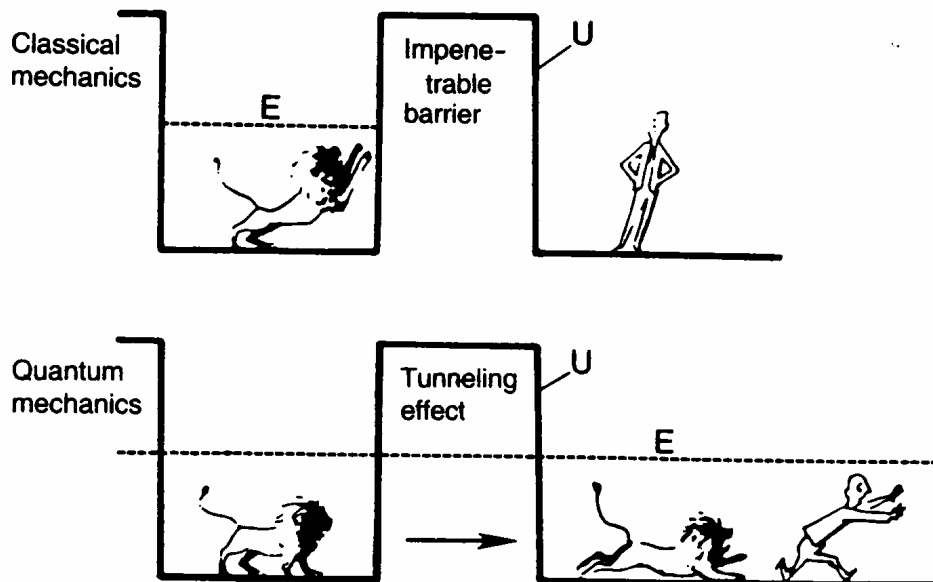


Fig. 1.3. The difference between classical theory and quantum theory. In quantum mechanics, an electron has a nonzero probability of tunneling through a potential barrier. (After Van Vleck; see Walmsley, 1987.)

where

$$k = \frac{\sqrt{2m(E - U)}}{\hbar} \quad (1.4)$$

is the wave vector. The electron is moving (in either a positive or negative direction) with a constant momentum $p_z = \hbar k = [2m(E - U)]^{1/2}$, or a constant velocity $v_z = p_z/m$, the same as the classical case. In the classically forbidden region, Eq. (1.2) has a solution

$$\psi(z) = \psi(0)e^{-\kappa z}, \quad (1.5)$$

where

$$\kappa = \frac{\sqrt{2m(U - E)}}{\hbar} \quad (1.6)$$

is the decay constant. It describes a state of the electron decaying in the +z direction. The probability density of observing an electron near a point z is proportional to $|\psi(0)|^2 e^{-2\kappa z}$, which has a nonzero value in the barrier region, thus a nonzero probability to penetrate a barrier. Another solution, $\psi(z) = \psi(0)e^{\kappa z}$, describes an electron state decaying in the -z direction.

Starting from this elementary model, with a little more effort, we can explain some basic features of metal–vacuum–metal tunneling, as shown in Fig. 1.4. The *work function* ϕ of a metal surface is defined as the minimum energy required to remove an electron from the bulk to the vacuum level. In general, the work function depends not only on the material, but also on the crystallographic orientation of the surface (see Section 4.2). For materials commonly used in STM experiments, the typical values of ϕ are listed in Table 1.1. (The work functions for alkali metals are substantially lower, typically 2–3 eV.) Neglecting the thermal excitation, the *Fermi level* is the upper limit of the occupied states in a metal. Taking the vacuum level as the reference point of energy, $E_F = -\phi$. To simplify discussion, we assume that the work functions of the tip and the sample are equal. The electron in the sample can tunnel into the tip and *vice versa*. However, without a bias voltage, there is no net tunneling current.

Table 1.1. Typical values of work functions. After *Handbook of Chemistry and Physics*, 69th edition, CRC Press (1988).

Element	Al	Au	Cu	Ir	Ni	Pt	Si	W
ϕ (eV)	4.1	5.4	4.6	5.6	5.2	5.7	4.8	4.8

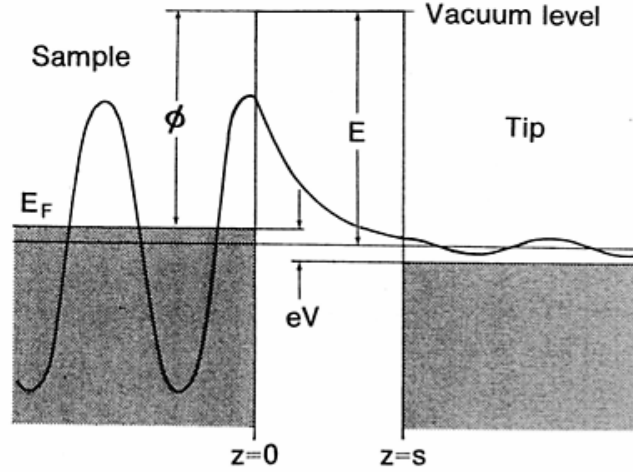


Fig. 1.4. A one-dimensional metal–vacuum–metal tunneling junction. The sample, left, and the tip, right, are modeled as semi-infinite pieces of free-electron metal.

By applying a bias voltage V , a net tunneling current occurs. A sample state ψ_n with energy level E_n lying between $E_F - eV$ and E_F has a chance to tunnel into the tip. We assume that the bias is much smaller than the value of the work function, that is, $eV \ll \phi$. Then the energy levels of all the sample states of interest are very close to the Fermi level, that is, $E_n \approx -\phi$. The probability w for an electron in the n th sample state to present at the tip surface, $z = W$, is

$$w \propto |\psi_n(0)|^2 e^{-2\kappa W}, \quad (1.7)$$

where $\psi_n(0)$ is the value of the n th sample state at the sample surface, and

$$\kappa = \frac{\sqrt{2m\phi}}{\hbar} \quad (1.8)$$

is the decay constant of a sample state near the Fermi level in the barrier region. Using eV as the unit of the work function, and \AA^{-1} as the unit of the decay constant, the numerical value of Eq. (1.8) is

$$\kappa = 0.51 \sqrt{\phi(\text{eV})} \text{\AA}^{-1}. \quad (1.9)$$

In an STM experiment, the tip scans over the sample surface. During a scan, the condition of the tip usually does not vary. The electrons coming to the tip surface, $z = W$, have a constant velocity to flow into the tip. The tunneling

current is directly proportional to the number of states on the sample surface within the energy interval eV , which are responsible for the tunneling current. This number depends on the local nature of the sample surface. For metals, it is finite. For semiconductors and insulators, the number is very small or zero. For semimetals, it is in between. By including all the sample states in the energy interval eV , the tunneling current is

$$I \propto \sum_{E_n = E_F - eV}^{E_F} |\psi_n(0)|^2 e^{-2\kappa W}. \quad (1.10)$$

If V is small enough that the density of electronic states does not vary significantly within it, the sum in Eq. (1.10) can be conveniently written in terms of the *local density of states (LDOS)* at the Fermi level. At a location z and energy E , the LDOS $\rho_S(z, E)$ of the sample is defined as

$$\rho_S(z, E) \equiv \frac{1}{\epsilon} \sum_{E_n = E - \epsilon}^E |\psi_n(z)|^2, \quad (1.11)$$

for a sufficiently small ϵ . The LDOS is the number of electrons per unit volume per unit energy, at a given point in space and at a given energy. It has a nice feature as follows. The probability density for a specific state, $|\psi_n|^2$, depends on the normalization condition: its integral over the entire space should be 1. As the volume increases, the probability density $|\psi_n|^2$ of a single state decreases; but the number of states per unit energy increases. The LDOS remains a constant. The value of the surface LDOS near the Fermi level is an indicator of whether the surface is metallic or insulating.

The tunneling current can be conveniently written in terms of the LDOS of the sample:

$$\begin{aligned} I &\propto V \rho_S(0, E_F) e^{-2\kappa W} \\ &\approx V \rho_S(0, E_F) e^{-1.025\sqrt{\phi} W}. \end{aligned} \quad (1.12)$$

The typical value of work function is $\phi \approx 4$ eV, which gives a typical value of the decay constant $\kappa \approx 1 \text{ \AA}^{-1}$. According to Eq. (1.12), the current decays about $e^2 \approx 7.4$ times per \AA .

The dependence of the logarithm of the tunneling current with respect to distance is a measure of the work function, or the tunneling barrier height (Garcia, 1986; Coombs and Pethica, 1986). In fact, from Eq. (1.12),

SEM (Scanning Electron Microscope)

TEM (Transmission Electron Microscope)

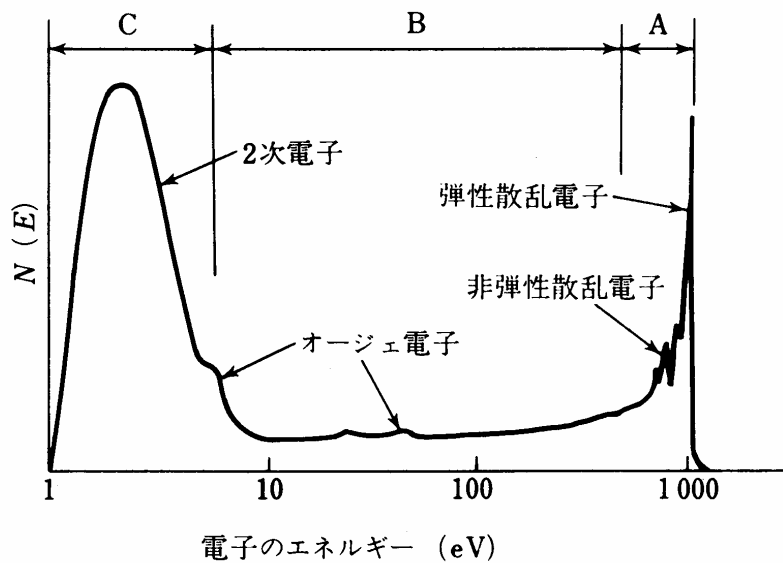
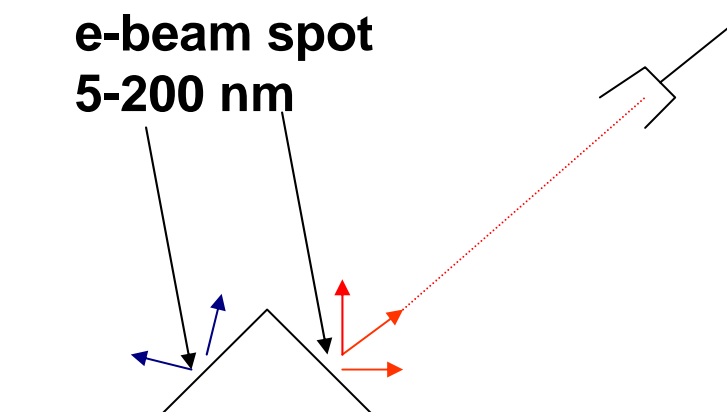
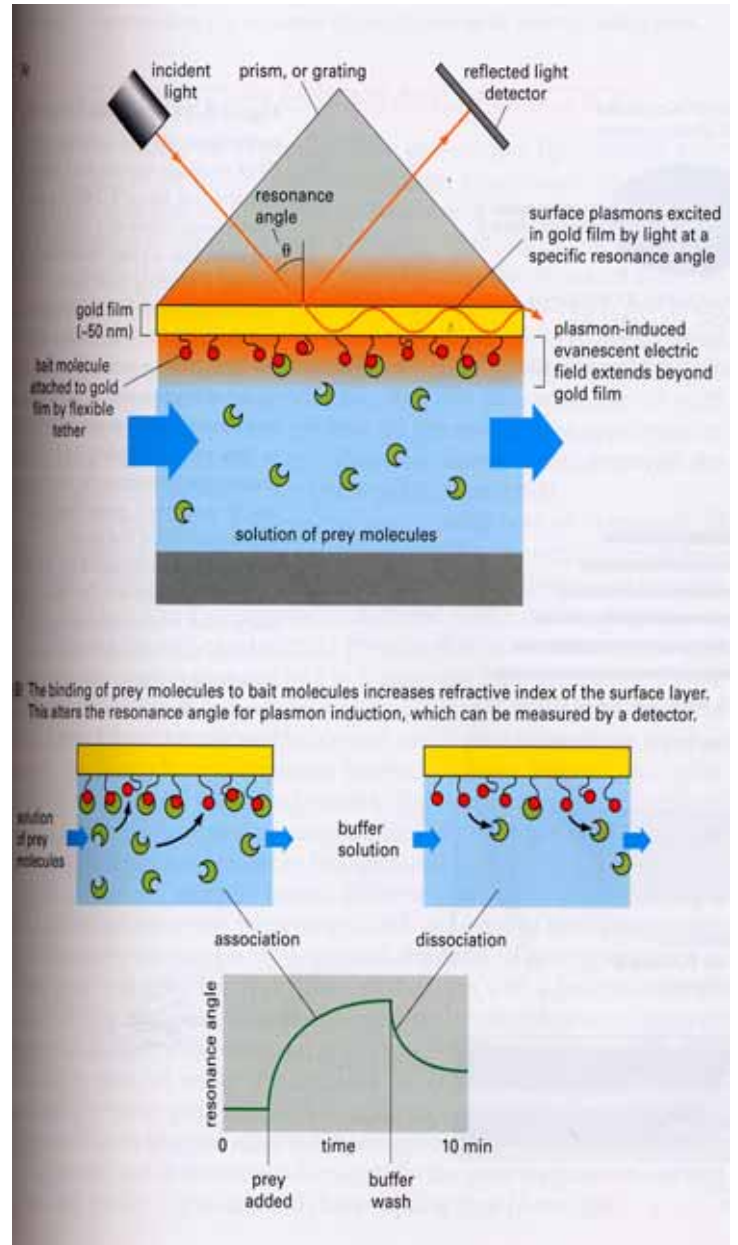


図 2.61 固体表面から後方に散乱または放出する電子のスペクトル (入射エネルギー1000eV)

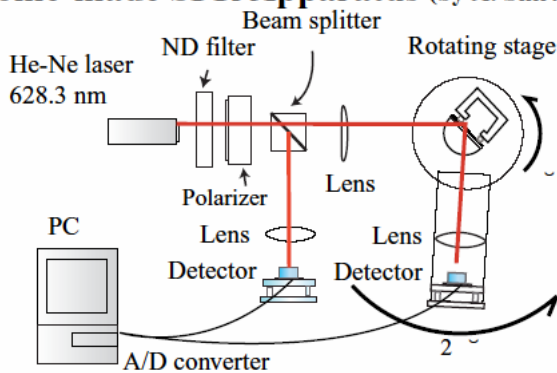


SPR (surface plasmon resonance)

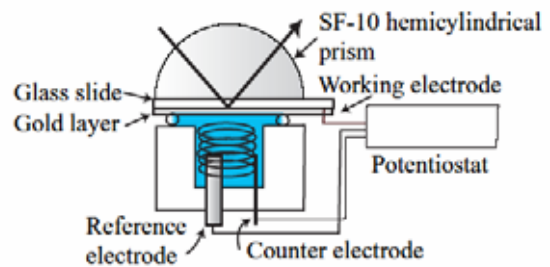
Ref:MBC



Home-made SPR Apparatus (by A. Shirakami)



Electrochemical Cell for SPR



Details of the Sample Setup

SF10 glass Prism
n matching oil
SF10 slide glass
MPS
Au film (50nm)
SAM

SPR principles

光による表面プラズモン(電荷密度波)の励起による共鳴

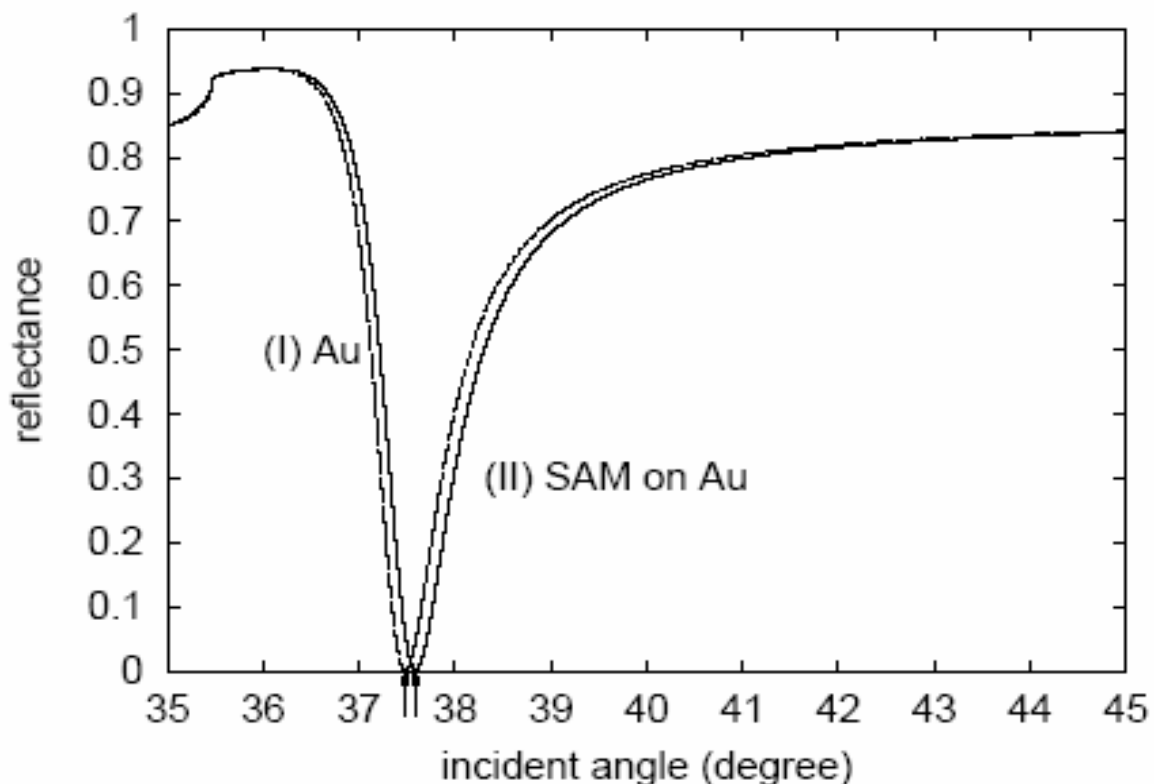
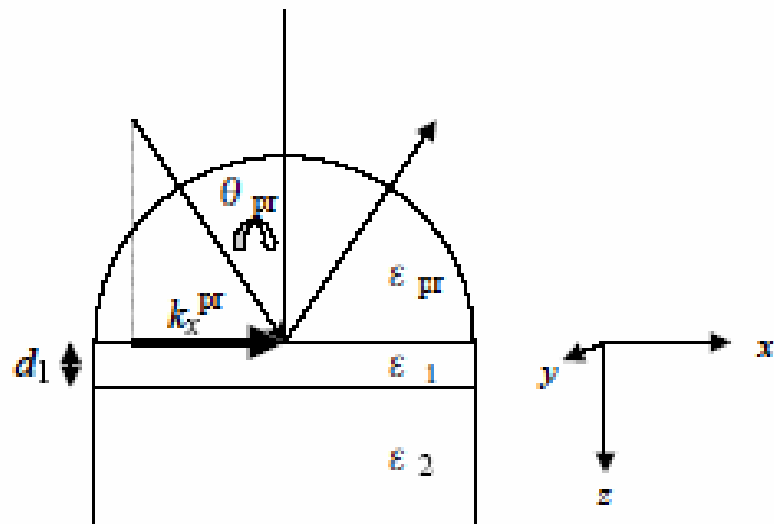
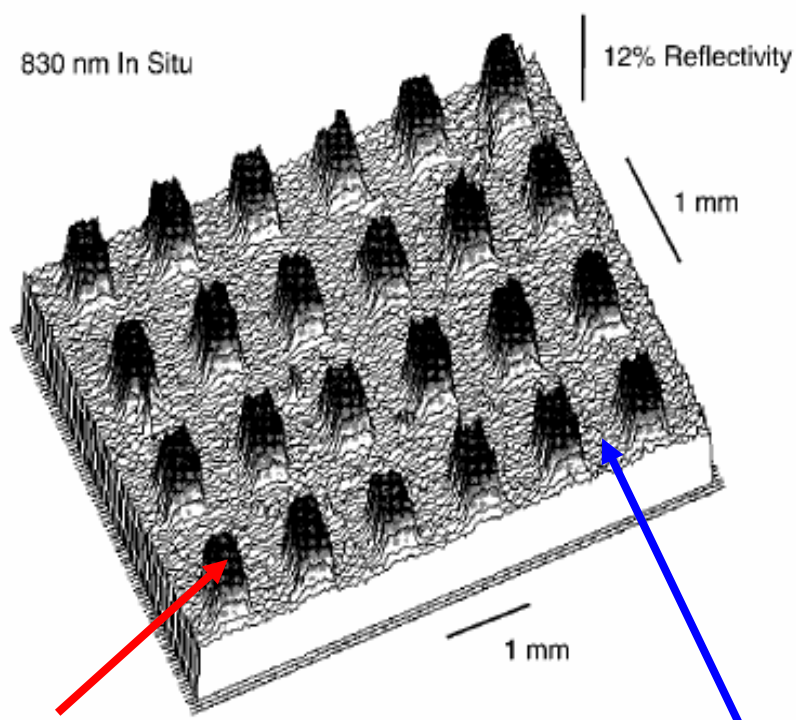


Figure 14: SPR curves for (I) the SF10 glass prism($n=1.723$)|Au($n + ik = 0.1726 + i3.4218$, 50nm)|Air($n=1.0$) and (II) the SF10 prism|Au(50nm)|SAM($n=1.61245$, 1nm)|Air systems.

Binary SAM on Au:
Surface Plasmon Resonance Sensor *DNA-Protein*
binding

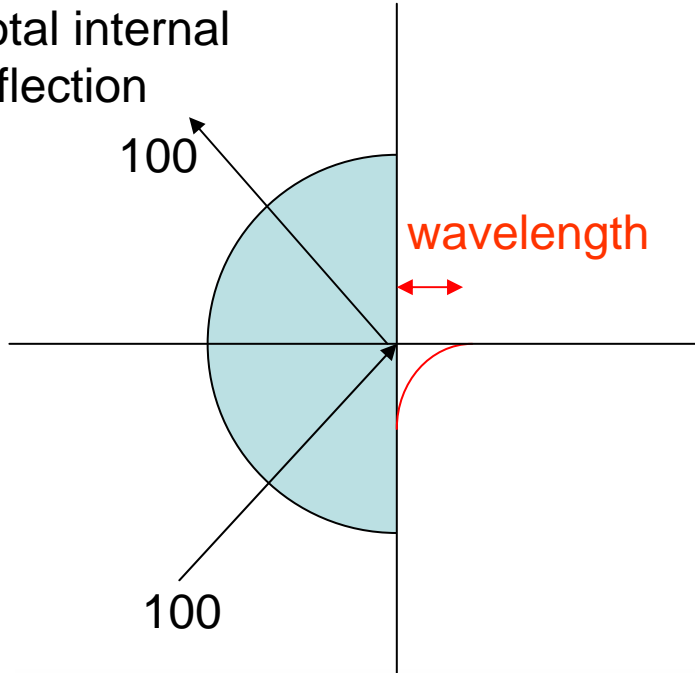


Single strand
DNA on Au
(5nm thick)
: Proteins bind
here

PEG Thiol on Au:
No Protein Adsorption

Nelson BP, Frutos AG, Brockman JM, et al. ANALYTICAL CHEMISTRY 71 (18):
3928-3934 SEP 15 1999

Total internal reflection



Evanescent wave

The transmitted wave can be written as

$$E'' = T_0 e^{i(k'' \cdot r - \omega'' t)} \quad (121)$$

$$= T_0 e^{i(k'' \sin \theta'' x + k'' \cos \theta'' z - \omega'' t)} \quad (122)$$

$$= T_0 e^{i(k'' \sin \theta'' x - \omega'' t)} e^{-k'' \sqrt{(n_1/n_2)^2 \sin^2 \theta - 1} z} \quad (123)$$

$$= T_0 e^{i \frac{n_2 \omega \sin \theta''}{c} x} e^{-i \omega'' t} e^{-\frac{n_2 \omega \sqrt{(n_1/n_2)^2 \sin^2 \theta - 1}}{c} z} \quad (124)$$

The transmitted light intensity decays as $e^{-\frac{2n_2 \omega \sqrt{(n_1/n_2)^2 \sin^2 \theta - 1}}{c} z}$. The decay length is the order of wavelength because $c/\omega = \lambda/2\pi$. The Poynting vector S in the z direction in the medium 2,

1分子イメージング

柳田敏雄、「生物分子モータ : ゆらぎと生体機能」
岩波物理の世界

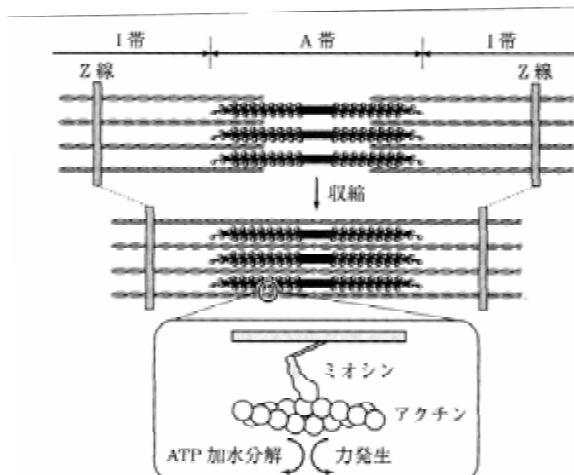


図 2.2 筋肉のスライディングモデル。筋の収縮はミオシンフィラメントとアクチンフィラメントがおたがいに滑ることによる。

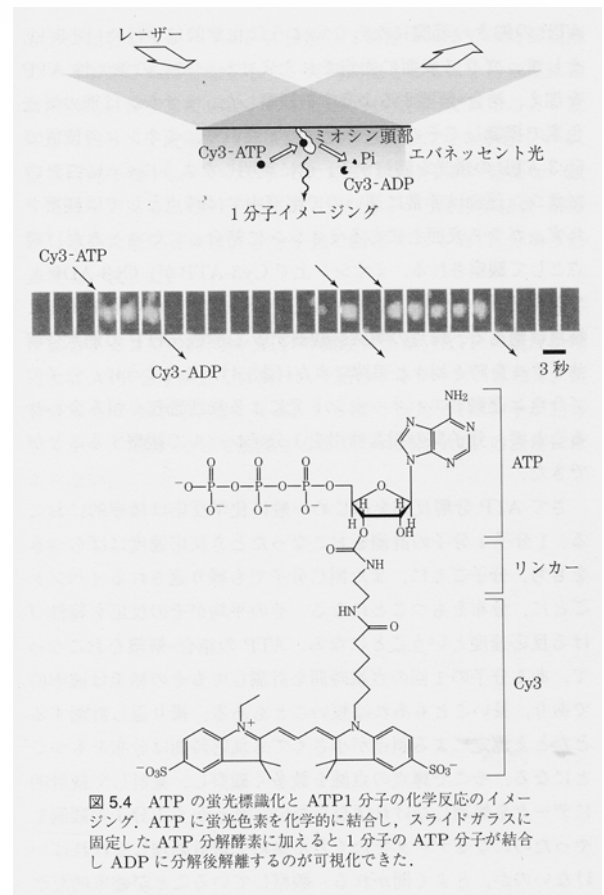


図 5.4 ATP の蛍光標識化と ATP1 分子の化学反応のイメージング。ATP に蛍光色素を化学的に結合し、スライドガラスに固定した ATP 分解酵素に加えると 1 分子の ATP 分子が結合し ADP に分解後解離するのが可視化できた。